Water Research X 25 (2024) 100275

Contents lists available at ScienceDirect

Water Research X

journal homepage: www.sciencedirect.com/journal/water-research-x

Application of organic silicon quaternary ammonium salt (QSA) to reduce carbon footprint of sewers: Long-term inhibition on sulfidogenesis and methanogenesis

Suwan Dai [a], Haixiao Guo [a], Yiming Li [a], Jiaqi Hou [a], Yufen Wang [a], Tingting Zhu [a], Bing-Jie Ni [b], Yiwen Liu [a,*]

[a] School of Environmental Science and Engineering, Tianjin University, Tianjin 300072, PR China
[b] School of Civil and Environmental Engineering, University of New South Wales, Sydney, New South Wales, 2052, Australia

ARTICLE INFO

Keywords:
Sulfide
Methane
Organic silicon quaternary ammonium salt (QSA)
Sewer corrosion
Biocidal effect
Organic loss

ABSTRACT

Sulfidogenic and methanogenic processes are undesirable in sewer management, yet the derived problems regarding organic losses are often neglected. Traditional chemical dosing methods aimed at sulfide and methane control commonly involve similar mechanisms of oxidation and/or precipitation. Moreover, previous focuses were centered on elevating control efficacy rather than investigating interactions between dosed chemicals and biofilms. In this work, organic silicon quaternary ammonium salt (QSA) of 75 mg-N/L was firstly applied in laboratory pressurized sewer reactors. After three dosing events, it took 20 days for sulfidogenic activities to recover to 50 % without further elevations. Meantime, methanogenic activities were stable ca. 11 % without significant inclinations to recover. Notably, consumption rate of chemical oxygen demand (COD) was suppressed to 50 % at most, and no microbial resistance to QSA but better control efficacy was observed. Characterizations of physicochemistry, microbial community and metabolism were conducted to elucidate mechanisms. Results showed that QSA was attached on sewer biofilms via electrostatic attraction to exert enduring control efficacy. Biofilms tended to become more hydrophobic and compact after QSA exposure. Microbial analyses indicated that relative abundances of microbes regarding hydrolysis, acidogenesis and methanogenesis were sharply decreased together with down-regulation of pivotal enzymatic activities. Additionally, denitrification batch tests initially suggested that the biodegradability of effluent was significantly enhanced, which ensured the safety of QSA dosing into sewers. Overall, results of this work were expected to lay a theoretical foundation on employing QSA to wastewater management.

1. Introduction

As an important municipal infrastructure, sewers transport sewage to wastewater treatment plants (WWTPs). Due to the anoxic condition, anaerobic microbes thrive in sewers, forming mature biofilms. Typically, sulfide and methane are originated from sulfate reducing bacteria (SRB) and methanogenic archaea (MA) in sewers, triggering corrosion and emission of greenhouse gases (He et al., 2023). Consequently, the government maintains sewer systems at high costs. Furthermore, both SRB and MA are heterotrophic microbes, causing a deficient chemical oxygen demand (COD) in sewage (Kobylinski et al., 2010). Thus, extra chemicals are required to ensure the performance of further wastewater treatment. Overall, suppression of sulfide and methane in sewers are extremely urgent.

So far, technologies for controlling sulfide and methane have been extensively investigated (Zhang et al., 2023). Particularly, chemical dosing is commonly employed and mainly includes sulfide oxidants, precipitation agents and biocides (Wang et al., 2023). Thereinto, sulfide oxidants and precipitation agents require constant dosing, incurring high costs. Biocides can exert enduring efficacy yet derived environmental problems are often neglected. For instance, advanced oxidation technologies such as peracetic acid inevitably oxidize raw organics in sewage, weakening the control performance and wasting COD (Wang et al., 2024). Also, adjusting the pH is needed when applying free nitrous acid (FNA) or free ammonia (FA) (Zuo et al., 2020). Moreover, biological resistance to biocides is frequently reported, contributing to more

* Corresponding author.
E-mail address: yiwen.liu@tju.edu.cn (Y. Liu).

https://doi.org/10.1016/j.wroa.2024.100275
Received 27 August 2024; Received in revised form 9 October 2024; Accepted 1 November 2024
Available online 1 November 2024

dosage. Furthermore, traditional chemicals are easy to be flushed away rather than retained in sewers to exert enduring effects. Regarding the research gaps, till now most of works have been concentrated on dosing chemicals in sewers without considering the impact on downstream WWTPs. Moreover, prior studies have revealed the COD consumption in the context of implementing chemical dosing or not (Kobylinski et al., 2007, 2008). Yet many studies about controlling sulfide or methane mainly focused on rates of sulfide and methane production rather than including COD consumption.

Quaternary ammonium salts (QA) are disinfectants and widely applied in water treatment (Liu et al., 2024). Compared to traditional QA, organic silicon quaternary ammonium salt (QSA) is competitive in long-term attachment, superior biocidal efficacy, environmental-friendliness, and practically non-toxic. Moreover, QSA inactivates microbes mainly by physically disrupting cytomembrane, lowering the risk of resistance (Vereshchagin et al., 2021). Regarding its application in relieving corrosion, a QSA-treated concrete achieved suppression on SRB for 28 days (Etim et al., 2020). However, QSA has never been applied in sewer systems and the potential inhibition mechanism has remained unclear yet.

To fill the knowledge gap, QSA was dosed into laboratory rising main reactors and this work aimed to: (1) assess the feasibility of dosing QSA to suppress sulfide/methane production and COD consumption in sewer systems; (2) dissect the inhibition mechanism from perspectives of physicochemistry, microbial community and metabolism; (3) elucidate the impact of QSA dosing on downstream denitrification process. The outcomes of this work are believed to lay a theoretical foundation for practically applying QSA to enhance sewer management.

2. Results and discussions

2.1. Impact of dosing QSA on biofilm activities

Fig. 1 Relative sulfide production rate (SPR) (A); Relative methane production rate (MPR) (B); and relative COD consumption rate (CCR) (C). The notation “Arrow (↓)” means a dosing event.

As displayed in Fig. 1, rates of SPR, MPR and CCR were determined. In Phase I, the pseudo-steady state was obtained where biofilm activities

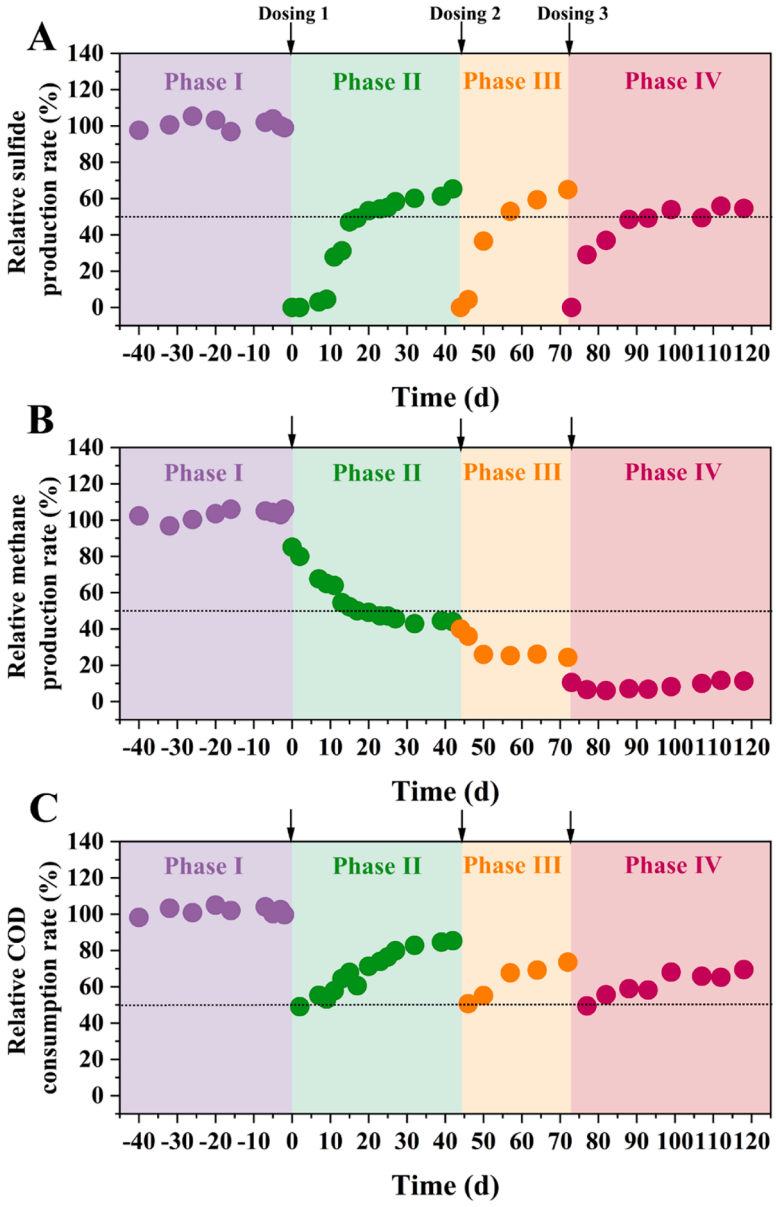

Fig. 1. Relative sulfide production rate (SPR) (A); Relative methane production rate (MPR) (B); and relative COD consumption rate (CCR) (C). The notation “Arrow (↓)” means a dosing event.

were similar in both reactors. In Phase II, after exposure, SPR was completely suppressed. A 9-day lag in SPR recovery was followed with a rebound to 50 %. However, such recovery was slowed after 20 days, reaching 65 % on day 42. Whereas, MPR witnessed a gradual decline from 85 to 44 % rather than recovery. Interestingly, such phenomenon could be attributed to the gradual permeation of QSA, shift of relevant microbes and attached QSA in biofilms, which was discussed further. Sewer biofilms are stratified where SRB resides in the superficial layer while MA in the deep (Zan et al., 2021). Thus, biocides firstly contacted SRB and then reached the deep zone to kill MA. Moreover, CCR fluctuated ca. 50 % in the first 10 days and then gradually increased to 85 % on day 42, corresponding to the recovery tendency of SPR.

In Phase III, SPR and CCR both recovered faster than Phase II. Specifically, no hysteresis phenomenon was observed during recovery and it took about 13 days for SPR to recover 50 %. Notably, MPR descended slowly in the first two days and finally stabilized ca. 25 %. Similar to Phase II, CCR was continuously recovered from 51 to 74 % during Phase III. Overall, the control efficacy of QSA on sulfide and methane was possibly time-dependent. By prolonging the exposure time, more QSA in aqueous solutions could be captured by biofilms and exert biocidal effects.

Phase IV was a replication of Phase III to assess the potential resistance. Interestingly, efficiencies of SPR, MPR inhibition and COD entrapment in Phase IV were even better than Phase II. Specifically, the time required to recover 50 % SPR in Phase IV was longer than Phase II (20 vs. 17 days). Moreover, SPR and MPR were stabilized ca. 50 and 11 % even 45 days after the third dosing event, respectively. After repeated dosing events, it was likely that biofilms were significantly weakened and more sensitive to biocides (Guo et al., 2023a). Also, no observation of resistance could be attributed to the long interval dosing events and unique biocidal mechanisms of QSA. Due to the superior efficacy compared to other biocides (Table S2), QSA was not required to be dosed frequently, avoiding the microbial adaption caused by continual dosing events. Moreover, the antimicrobial resistance to biocides mainly results from more EPS secretion or passivating enzyme formation (Jaillard et al., 2017). Yet QSA mainly kills bacteria via physical contact and long-term attachment, killing the bacteria before adaption (Bai et al., 2019). In future studies, long-term experiments or repeated exposures (low dosage but high frequencies) could be implemented to further assess the risk of antimicrobial resistance to QSA.

2.2. Alterations of physiochemical characterizations after QSA dosing

2.2.1. Morphology and functional groups

Fig. 2 SEM images and EDS mapping of biofilms in R1 (A), R2 (B); Relative content of major elements in biofilms (C); FTIR spectra of biofilms (D) and EPS (E); Second derivative curve fitting of S-EPS and TB-EPS in the amide I region (1700–1600 cm^{-1}) (F).

As displayed in Fig. 2A and B, biofilm cells were transformed from smooth spheres into agglomerated structures, indicating cell death. The EDS mapping showed that Fe and Na (mainly intracellular) were widely distributed among biofilm-R1 (Campos et al., 2021). Conversely, biofilm-R2 exhibited increased Si but decreased Fe and Na signals. Fig. 2C provided the relative content of five key elements. The content of Si, Fe and Na corresponded to the mapping intensities. Besides, the increased C content was likely due to retained QSA in biofilms while decreased N content suggested the release of intracellular protein. Furthermore, Fig. S2 showed that on day 40 the content of Si and C in R2 were still higher than R1, implying the tight combination between QSA and biofilms. Therefore, it could be inferred that after exposure, QSA was fully captured by the biofilm matrix. Consequently, QSA disintegrated cells and resulted in leakage of intracellular matter. Also, QSA exerted a 'flocculation' effect on biofilms.

The FTIR spectra of biofilms and extracted EPS were displayed in Fig. 2D and E. Overall, the functional groups were classified into five categories (summarized in Table S3) (Li et al., 2021). As for biofilms (Fig. 2D), intensified peaks at 2923 and 2853 cm^{-1} were assigned to -CH_2 in QSA. An obvious peak at 872 cm^{-1} was determined to be O-P-O in nucleic acids, resulting from cell rupture. Besides, a weak peak at 916 cm^{-1} was attributed to Si-CH_3. Interestingly, R2–42 d and R2–46 d shared the similar types of functional groups, indicating the enduring attachment of QSA on biofilms. As for EPS, Fig. 2E indicated that

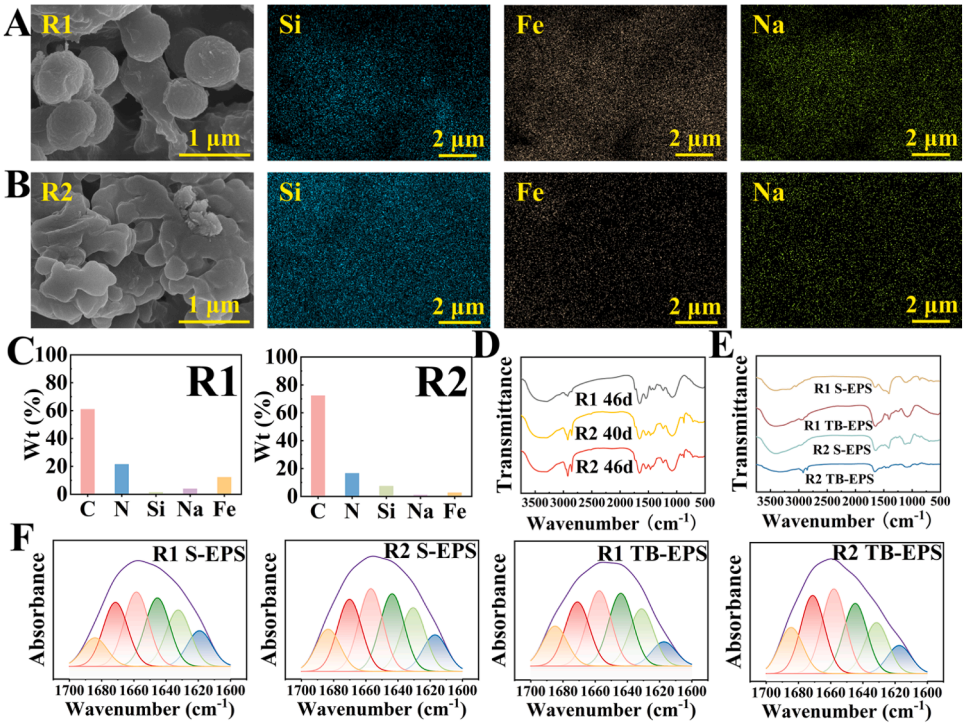

Fig. 2. SEM images and EDS mapping of biofilms in R1 (A), R2 (B); Relative content of major elements in biofilms (C); FTIR spectra of biofilms (D) and EPS (E); Second derivative curve fitting of S-EPS and TB-EPS in the amide I region (1700–1600 cm^{-1}) (F).

variations in functional groups bore much resemblance with those of biofilms. Notably, peaks of alkyl or silane were barely found in R2 S-EPS, hinting that little QSA was retained in the liquid phase. However, distinct peaks of alkyl were detected in TB-EPS of R2, implying that biofilm was a sink for QSA. Additionally, the increment of -OH, amide I, and C—O-C intensities in R2-S-EPS were related to release of humic substances, protein and polysaccharides, respectively.

Furthermore, secondary structure of proteins was analyzed. According to Fig. 2F and Table S4, the proteinic conformation of biofilm was altered after QSA treatment. Notably, the value of α-Helix/(β-sheet+ random coil) was increased to 69.85 % in TB-EPS, while it was slightly decreased to 58.54 % in S-EPS. Hence, it could be speculated that QSA exposure would tighten the biofilms, i.e., in line with the SEM observations (You et al., 2017). Such effect might be beneficial to retaining QSA in biofilms or strengthening the mass transfer limit.

2.2.2. Overall analysis of EPS

Fig. 3 Concentrations of protein (A), polysaccharides (B) and PN/PS (C); Variations of TSS in effluent during Phase II (D); Distributions of generic species related to hydrolysis, acidification, sulfidogenesis and methanogenesis processes (E).

To further explore the impact of QSA dosing on EPS, variations of protein (PN) and polysaccharides (PS) in EPS were determined. As presented in Fig. 3A and B, the content of total PN and PS in R2-biofilm were increased to 325.04 and 44.79 mg/gVSS, implying the self-protection of biofilm to biocides (Zhu et al., 2023). Also, the surge of PN and PS content in S-EPS indicated the release of intracellular matter (Wang et al., 2022). Moreover, the PN/PS ratio in Fig. 3C was significantly elevated from 4.09 to 17.16, suggesting the aggregation and hydrophobicity of biofilms (Liu et al., 2023).

The EEM spectra was employed to determine types of dissolved organic matter in EPS. After QSA treatment, fluorescence peaks of biodegradable organics (microbial byproducts-like substances) in R2 were conspicuously intensified (Fig. S3) (Li et al., 2020). Besides, peaks belonging to tyrosine-like, tryptophan-like, fulvic acid-like and humic acid-like substances in R2 were also detected, corresponding to the FTIR spectra. It could be conjectured that the biodegradability of effluent was enhanced after QSA exposure.

The effluent TSS was an index characterizing the stability of biofilms. In Fig. 3D, TSS of R2 underwent a U-type curve variation. In the first two days, due to overstress exerted by QSA, cells on the surface layer were killed and superficial biofilms were inevitably disintegrated. With the deeper penetration of QSA, biofilms were inclined to become compact. Consequently, the loss of biomass was declined, better retaining QSA in biofilms and ensuring the long-lasting control effect.

2.3. Effects of QSA dosing on microbes

To elucidate the response of microbes to QSA treatment, biofilm samples were extracted and sequenced. The rarefaction curve and Venn diagram in Figs. S4 and S5 suggested the reliability of sequencing data and alternations in microbial species. Variations in Sobs, Ace, Shannon and Simpson indices (Fig. S6) meant the reduced richness and diversity of microbial community.

According to Fig. S7, microbial compositions were differentiated in both reactors. On a phylum level, the relative abundance of alkane-resistant *Proteobacteria* and *Campilobacterota* were significantly increased, resulting from the alkylation of biofilm (Unnikrishnan et al., 2024). Additionally, abundances of other phyla involved in degrading organics and fermentation (e.g. *Firmicutes, Bacteroidota, Chloroflexi,*

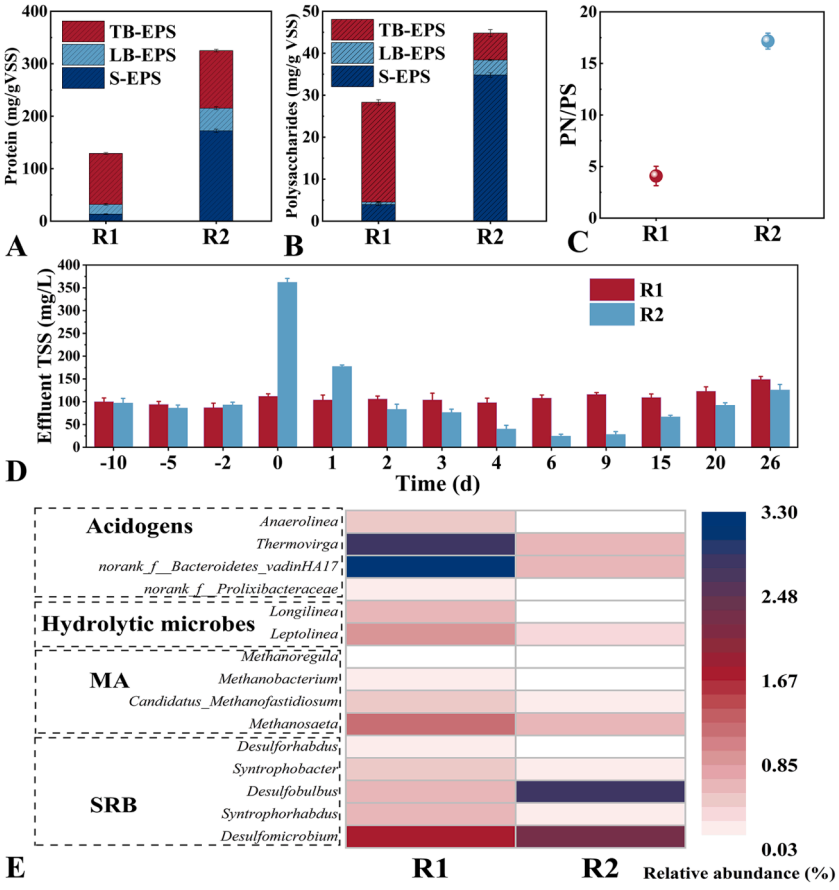

Fig. 3. Concentrations of protein (A), polysaccharides (B) and PN/PS (C); Variations of TSS in effluent during Phase II (D); Distributions of generic species related to hydrolysis, acidification, sulfidogenesis and methanogenesis processes (E).

Synergistota) were obviously decreased, corresponding to the declined CCR in Fig. 1.

At the genus level, the heatmap shown in Fig. 3E showed that six genera affiliated with acidogenesis and hydrolysis were significantly suppressed. Thus, available COD (e.g., acetic acid) which could be directly utilized by SRB and MA was insufficient. Consequently, SRB would outcompete MA for carbon utilization, causing faster recovery of SPR compared to MPR. As to MA, abundances of the top four genera were all inhibited in R2. Specially, the predominant genus *Methanosaeta* was declined from 1.21 to 0.61 %. Regarding SRB, abundances of *Syntrophorhabdus* and *Syntrophobacter*, which form mutualistic relationship with *Methanosaeta*, were decreased in R2, corresponding to the recession of *Methanosaeta* (Usman et al., 2023). Notably, abundances of other dominant genera, such as *Desulfobulbus* and *Desulfomicrobium* were increased while *Desulforhabdus* was decreased. Totally, QSA dosing shifted the metabolic pathway of sulfide production in biofilms. Previous studies also witnessed the enrichment of *Desulfobulbus* after dosing biocides (Guo et al., 2023a). However, since SPR was significantly suppressed and the richness and diversity of biofilms were decreased, the absolute abundance of SRB was likely decreased.

As shown in Fig. S8, activities of six key enzymes were inhibited after QSA exposure. Thereinto, activities of enzymes concerning hydrolysis, acidogenesis and methanogenesis were down-regulated, conforming to the decreased abundances of relevant microbes. Interestingly, APS reductase and sulfite reductase involved in reducing sulfate were also suppressed to 60 and 56.67 % of R1, further solidifying the deduction of decreased SRB. Overall, QSA was detrimental to the physiological process of methanogenesis and sulfidogenesis. The suppressed activities of enzymes were possibly due to the massive death of microbes and potential interactions between enzymes and QSA.

2.4. Environmental risks of QSA to downtream denitrification

Fig. 4 Effects of sewer effluent with QSA on denitrification of nitrite (A) and nitrate (B). The notation "x- dilution" meant the effluent was diluted with deionized water for appointed times; "no C" meant no extra COD stock solution. Asterisks (*) manifest significant differences compared to the control (one-way ANOVA, ns, $p > 0.05$, * $p < 0.05$, ** $p < 0.01$).

Biocides commonly had a merit of enduring inhibition on sewer biofilms compared to mild chemicals. However, concerns regarding the safety and environment-friendliness of biocides were often raised.

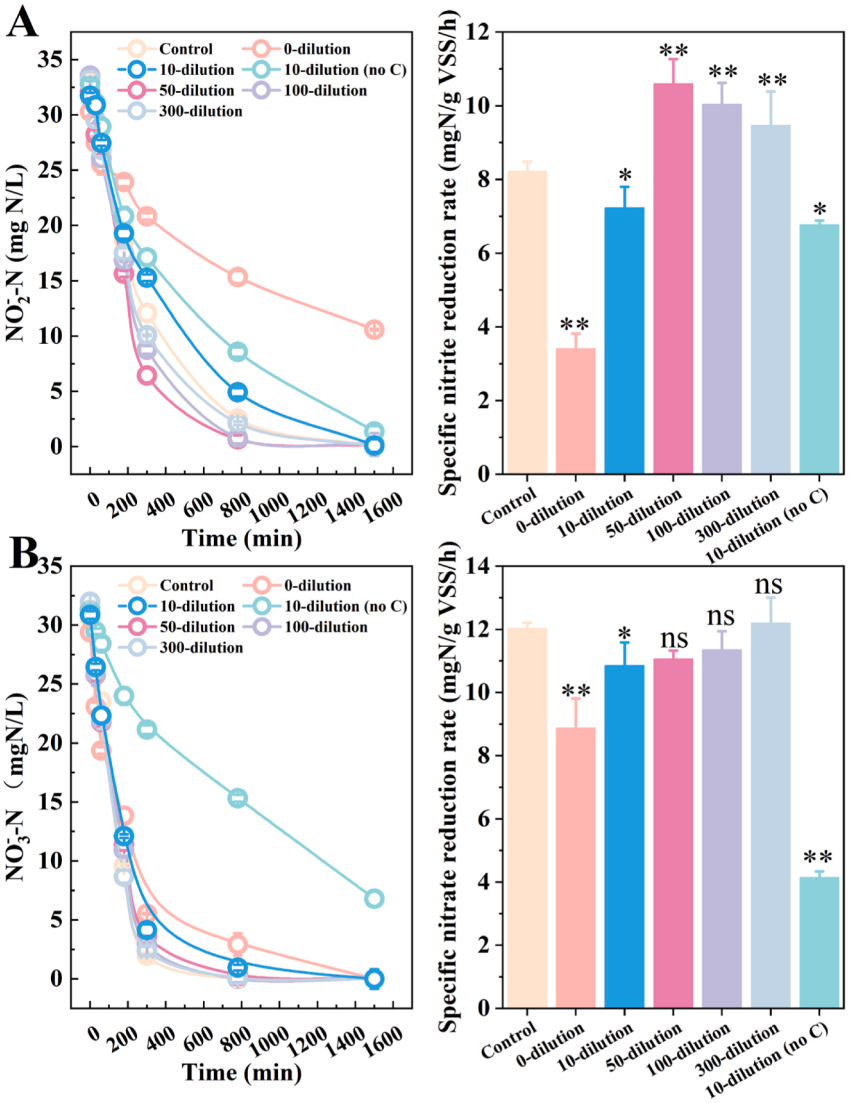

Fig. 4. Effects of sewer effluent with QSA on denitrification of nitrite (A) and nitrate (B). The notation "x- dilution" meant the effluent was diluted with deionized water for appointed times; "no C" meant no extra COD stock solution. Asterisks (*) manifest significant differences compared to the control (one-way ANOVA, ns, $p > 0.05$, * $p < 0.05$, ** $p < 0.01$).

Specifically, some biocides were acutely toxic to humans and detrimental to wastewater treatment units. Therefore, the effect of QSA on downstream WWTPs (i.e., denitrification process) was investigated. Herein, varied times of dilution (0–300 folds) were set to mimic the transport of QSA in real sewer systems (Jiang et al., 2013).

As displayed in Fig. 4, when QE was exposed to SBR sludge without dilution, denitrification process was negatively affected. In detail, the specific reduction rate of nitrite and nitrate were reduced from 8.23 to 3.41 and 12.03 to 8.88 mg-N/gVSS/h. However, such inhibition was significantly relieved when QE was diluted over 10 times. Ideally, on the condition of 300 folds dilution, both rates of nitrite and nitrate removal were higher than the control group (nitrite: 4.55 vs. 3.95 mg-N/gVSS/h; nitrate: 5.85 vs. 5.77 mg-N/gVSS/h). Interestingly, a "hormesis effect" was observed here. It might be attributed to the stress reaction of activated sludge, where EPS secretion was elevated and adaption to QSA was formed. Also, QSA might be conducive to electron transfer and metabolic activity, requiring further investigations (Xu et al., 2023).

To reveal the bioavailability of QE, two groups of 10 folds diluted effluent were set. One was supplemented with 300 mg-COD/L (C/N = 10) while the other was not. Theoretically, the C/N ratio of completely denitrifying nitrate and nitrite is 2.86 and 1.71, respectively (Yin et al., 2024). Thus, 10-dilution of the effluent without extra COD should have ensured a carbon-limit condition, yet in this case nitrite could achieve nearly complete degradation while nitrate was removed by 77.3 % after 1500 min. All the above results suggested that additional energy in the effluent was utilized for denitrification. The better nitrite degradation efficiency could be explained by the more requirements of electron donors (COD) for nitrate reduction, compared to nitrite. With prolonged time, nitrate would be further removed. Thus, it could be inferred that additional carbon source (e.g. PN, PS) in QSA-containing effluent was biodegradable for denitrification, corresponding to the EEM spectra. To the best of our knowledge, this is the first report confirming the

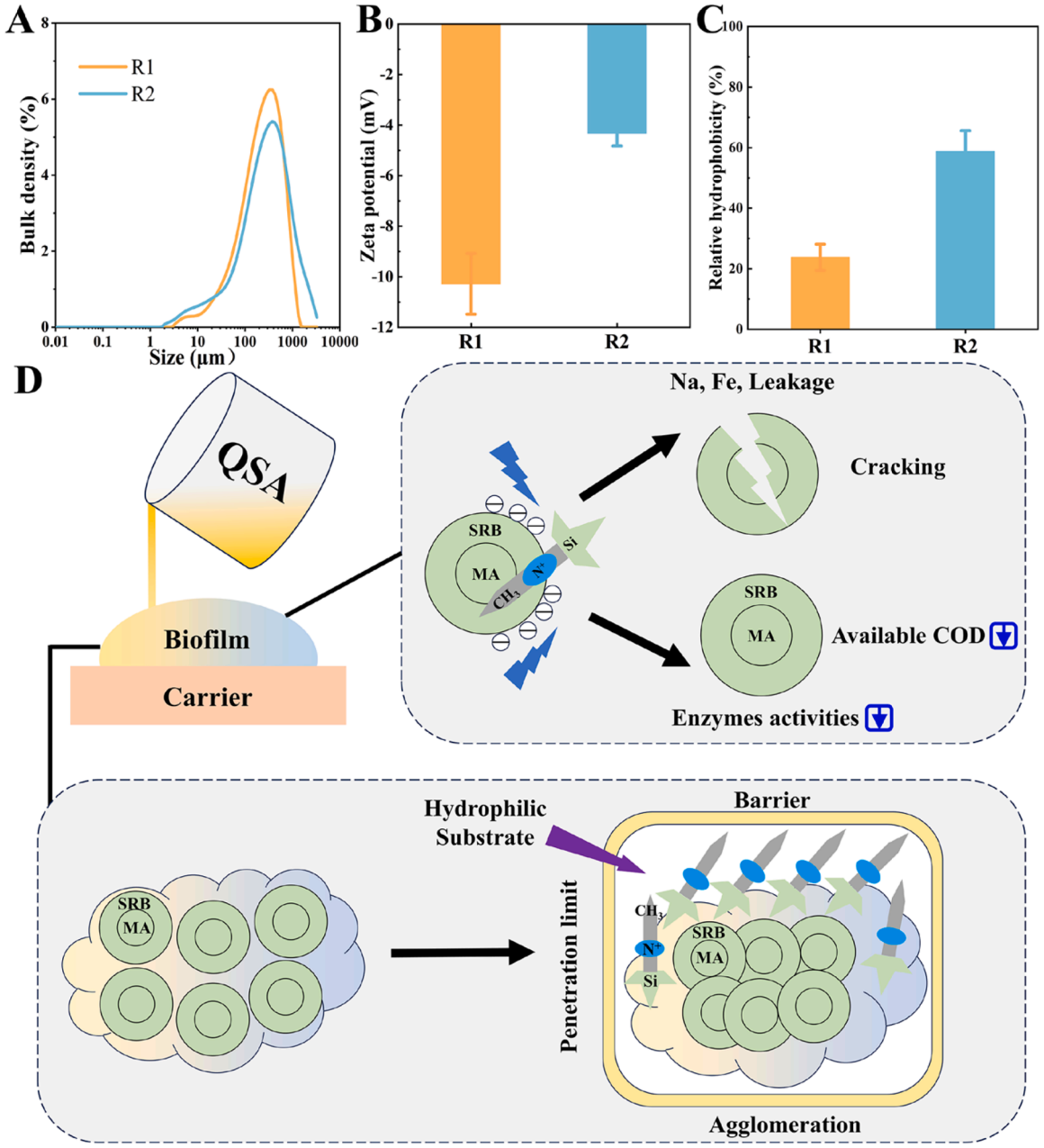

Fig. 5. Proposed mechanism of QSA inhibition on sulfide and methane production: Distribution of particle size (A); Zeta potential (B); Relative hydrophobicity (C); Proposed Mechanism (D).

feasibility of employing broken biomass from upstream sewer biofilms to supply downstream treatment.

2.5. Mechanism

Fig. 5 Proposed mechanism of QSA inhibition on sulfide and methane production: Distribution of particle size (A); Zeta potential (B); Relative hydrophobicity (C); Proposed Mechanism (D).

To comprehensively elucidate the mechanism, more characterizations were conducted. According to Fig. 5A, the Dx (50) and Dx (90) of biofilms were increased to 290 and 1030 μm, respectively, corresponding to the decreased TSS. The larger particle size of sludge possibly led to limited substrate transfer and intensified electron competition inside sludge flocs (He et al., 2024). It was likely that such limitation and competition also occurred in R2-biofilm. Thus, MA residing in deeper zone was overwhelmed by SRB and partly died from starvation. Such process was possibly progressive, corresponding to the gradual declination of MPR and decreased abundances of syntrophic SRB. Zeta potential could reflect the stability of particles. According to Fig. 5B, the mean zeta potential was higher in R2-biofilm than R1-biofilm, which was owing to the charge neutralization between negatively charged bacteria and positively charged QSA. Since QSA is cationic, electrostatic attraction occurs when it is exposed to biofilms, leading to enrichment of QSA in the biofilm matrix. Meanwhile, in Fig. 5C, the relative hydrophobicity of R2-biofilm was increased from 23.8 to 58.8 %, complying with the elevated PN/PS and decreased zeta potential (Wei et al., 2018). The increased hydrophobicity was ascribed to hydrophobic alkane chains on QSA or exposed hydrophobic groups of intracellular matter. Since the hydrophobic alkane groups were significant even after 40 days, QSA was inferred to be firmly combined with biofilms and the hydrophobicity was also retained. Thus, hydrophilic substrate such as sulfate is difficult to bypass the hydrophobic layer on R2-biofilm, partly explaining the slow recovery of SPR and MPR.

Based on the above discussions, the mechanism could be proposed as followed: Firstly, QSA contacted the superficial bacteria such as SRB. Under the stress of charge neutralization, cytomembranes of microbes were disrupted with intracellular matter leaked. Simultaneously, enzymes responsible for hydrolysis and acidogenesis were suppressed, leading to COD starvation. Then SRB outcompeted MA for COD utilization. The nutrient limitation in biofilm might also promote the adhesion effect, increasing the hydrophobicity and compactness of biofilm (Du et al., 2022). Due to electrostatic attraction, QSA was largely enriched in the biofilm and difficult to elute. With prolonged time, QSA penetrated into deep layers, further killing MA. Moreover, the structure of biofilms became more compact and hydrophobic, intensifying the limited substrate transfer and better retaining the adsorbed QSA. After repeated dosing events, more QSA were expected to be accumulated in biofilms with no resistance and better control efficacy.

3. Implications

This work successfully suppressed sulfide and methane by dosing QSA. Particularly, MA was enduringly suppressed without obvious recovery. Moreover, the newly introduced indicator CCR effectively assessed the biofilm activities. Overall, the superior efficacy of QSA avoided frequent dosing and microbial resistance, saving much costs. Besides, the underlying mechanism was investigated, demonstrating that attachment of QSA on biofilms ensured the long-lasting control efficiency. In contrast, traditional chemicals are easy to elute from biofilms, resulting in lower efficiency. Furthermore, this work innovatively confirmed the safety of dosed QSA and bioavailability of damaged biomass, offering a comprehensive perspective for wastewater management. For practical applications, some points should be addressed. Firstly, a prolonged exposure time and multiple dosing sites are suggested to ensure the sufficient adsorption of QSA on biofilms. Secondly, an intermittent dosing strategy is advised to implement. Eventually, QSA is proposed to be dosed at upstream sewers (i.e., manholes or pumping stations) at midnight to minimize the dilution of flowing sewage. Actually, hot spots of corrosion are commonly reported at upstream sites since nutrients are abundant therein (Zuo et al., 2024).

As for QSA, USEPA deemed it as practically non-toxic chemicals (USEPA, 2007). Moreover, electrostatic attraction occurred between QSA and bacteria. Consequently, most QSA would be enriched in sewer biofilms or sediments without being flushed away, relieving environmental risks. Even if QSA was partly escaped into liquid phases, the gradual hydrolysis of itself would forfeit bactericidal abilities (Chen et al., 2022). As to the ultimate fate, QSA might partly undergo aerobic biological degradation after entering WWTPs. Recently, ester bonds have been introduced into QA to enhance its biodegradability during aerobic treatment (Zhou et al., 2024). It should be noted that although QSA is considered safe herein for denitrification after the self-dilution of sewer, future studies are warranted to comprehensively evaluate its impact on the overall wastewater system (e.g., the anaerobic digestion). In fact, there have already been some studies applying QA to enhance the dewatering properties of digestion sludge and promote short chain fatty acid accumulation. (Liu et al., 2024; You et al., 2024). Furthermore, more benefits of dosing QSA could be uncovered. For instance, disinfection effect of QSA is beneficial to weakening the spread of COVID-19 in sewers, strengthening the adsorption capacity of biofilm to capture hydrophobic microplastics in sewage and so forth (Li et al., 2023; Subair et al., 2024). Overall, this work provided a theoretical insight into the feasibility of applying QSA in the wastewater infrastructure and more possibilities are expected in future studies.

4. Conclusions

This work comprehensively investigated the feasibility of dosing QSA to control sulfide and methane in sewer biofilm with following conclusions drawn:

- QSA effectively suppressed sulfidogenesis and methanogenesis and COD consumption of sewer biofilm. The control efficacy could be enhanced by prolonging exposure time or intermittently dosing. Microbial resistance to QSA was not built herein.
- QSA dosing reshaped the structure of microbial community. Key enzymes regarding to sulfidogenesis and methanogenesis metabolisms were inhibited.
- Long-term attachment of QSA on biofilm was mainly achieved via electrostatic attraction, significantly relieving recovery of biofilm activities.
- Mechanism analyses indicated that the alteration in surface charge and hydrophobicity of biofilm led to cellular rupture and flocculation. Consequently, Potential mass transfer limit and enduring QSA attachment contributed to the long-term efficacy.
- The “self-dilution” effect of sewer and attachment of QSA on biofilms relieved the threat to downstream denitrification process. Leaked biomass from biofilm could be utilized as supplementary carbon sources.

5. Materials and methods

5.1. Setup and operation of sewer reactors

Two identical reactors (Fig. S1, namely R1 and R2) were established to simulate the conditions in rising mains. R1 was selected as the control group while R2 was the experimental group. Each reactor was air-tight, with a total volume of 0.75 L, a diameter of 80 mm and a height of 149 mm. Plastic carriers (K2, 15 mm diameter) were fixed on four rods inside the reactors to provide additional growth area for biofilm and allow the harvesting of intact biofilms. The total area of biofilm in each reactor was approximately 0.05 m^2, ensuring an A/V ratio of 67 m^2/m^3.

Reactors were fed with real domestic wastewater containing

200–350 mg COD/L, 25–35 mg SO_4^{2-}-S/L and sulfide < 2 mg-S/L (Tianjin, China). The wastewater was stored in a refrigerator at 4 °C to minimize the changes of composition. Then, it was preheated to 20 °C and pumped into reactors. The feeding patterns were composed of 4 pumping events every day, with 0.75 L wastewater per event, leading to a hydraulic retention time of 6 h Moreover, the reactors were stirred at 200 rpm to mimic a common shear force in the real sewer systems.

The overall experiments lasted for 158 days, consisting of four phases (Table S1). To cultivate mature biofilms and establish the pseudo steady-state conditions, reactors were monitored for 40 days before dosing QSA (Phase I, day −40 to −1). R1, as the control group, was all along operated under the same regime as Phase I. According to our preliminary experiment (data not shown), the concentration of QSA dosed in this work was determined as 75 mg-N/L. During Phase II (day 0 to 44), R2 was drained off and injected with QSA for 5 min on day 0. After exposure for 12 h, R2 was evacuated and refilled with fresh wastewater for 30 min to minimize the effect of residual QSA. To investigate the effect of exposure time on controlling sulfide and methane, a shortened exposure time of 6 h was applied on day 45 during Phase III (day 45 to 72). Eventually, the third dosing event on day 65 during Phase IV (day 73 to 118) was a replication of Phase III to evaluate whether biofilms would build resistance to QSA after previous two dosing events.

5.2. Batch tests

Batch tests were implemented to assess the biological activities of sewer biofilms during the whole experiment, with intervals varying between 1 and 7 days. Specifically, both reactors were firstly drained off and refilled with fresh wastewater for 15 min to achieve a complete substitution of substrate. Afterwards, 10 mL of liquid samples were harvested with 0.22 μm filters at 0, 20, 40, 60 min for further analyses of sulfide, methane and SCOD. Then, three key parameters, including sulfide production rate (SPR), methane production rate (MPR), and SCOD consumption rate (CCR) were obtained through liner regression calculations. Specifically, concentrations of sulfide, methane and SCOD were measured and liner fitting was applied to obtain the modelled slope of curve. The slope was then determined as the activity and activity ratio of R2/R1 was defined as the relative activity. To minimize the disturbance of varied concentrations of real wastewater, SPR, MPR and CCR were presented as relative activities (i.e., R2/R1, %) (Yan et al., 2020).

5.3. Physiochemical characterizations of biofilms after QSA dosing

To better illustrate the impact of QSA dosing on sewer biofilms, a series of characterizations were conducted. On day 40 (Phase II) and 46 (Phase III), biofilm samples were extracted from reactors for observing morphology, analyzing functional groups and microbial sequencing. To further elucidate the biocidal mechanism, carriers of R1 were harvested and batch experiments of QSA exposure were conducted (Text S1). After exposure to QSA, microbial extracellular polymeric substances (EPS) were extracted from biofilms using a modified heating method (Guo et al., 2023b). Concentrations of protein (PN) and polysaccharides (PS) in EPS were determined via colorimetric methods. The EEM fluorescence was applied to observe the variations of organic components in different layers of EPS (Baker, 2002). The transformation of microstructure was characterized by scanning electron microscope (SEM). Also, relative content and distribution of elements on biofilms were detected by energy disperse spectroscopy (EDS) mapping. Fourier transform infrared spectrometer (FTIR) was employed to compare the functional groups of biofilms and extracted EPS. Furthermore, to gain insight into the secondary structure of protein, amide I region (1700–1600 cm^{-1}) of FTIR spectra was processed by Peakfit. The size of biofilm was analyzed by a laser diffraction particle size analyzer (Mastersizer 3000, Malvern, UK). The zeta potential of biofilm was detected using a Zetasizer (Litesizer 500, Anton Paar, Austria). The hydrophobicity of biofilm was determined according to a n-Hexadecane method (Wang et al., 2014).

5.4. Analyses of microbial community and key enzymes

Biofilm samples from carriers were collected for microbial analyses. The DNA was extracted using a Fast DNA Spin Kit for Soil (Major Biotech, Shanghai, China). Then, Illumina Miseq sequencing of 16S rRNA was applied to reveal the compositions of microbial community (Text S2). The 16S rRNA was amplified with the forward primer 515FmodF (5′-GTGYCAGCMGCCGCGGTAA-3′) and 806RmodR (5′-GGACTACNVGGGTWTCTAAT-3′), targeting the hypervariable V4 region of the bacteria domain.

Enzymes commonly catalyze the reactions involved in biological metabolism. Herein, six enzymes which are related to hydrolysis, acid-formation, sulfidogenesis and methanogenesis were extracted. The activities of those enzymes were further determined in line with protocols summarized by Guo et al. (Guo et al., 2023a).

5.5. Assessment of environmental risks

Upon the termination of QSA exposure in Phase III, the effluent of R2 was harvested. Then, batch tests were carried out to evaluate the potential risks caused by QSA-containing effluent (QE) to downstream WWTPs. Herein, the denitrification process was selected as an example. Briefly, QE of different dilution times were mixed with nitrogen source and activated sludge in serum bottles. Liquid samples were withdrawn at predetermined intervals to analyze concentrations of nitrite and nitrate. Particularly, to ascertain whether the QE could be partly utilized by denitrification microorganisms, one group was set where QE was diluted to 10 times without adding additional COD. Details regarding the batch tests were shown in Text S3.

5.6. Other analytical methods

TSS and VSS were determined using a standard method. Dissolved sulfide was measured using the methylene blue method. A gas chromatography equipped with flame ionization detector (GC-FID) was employed to measure dissolved methane based on the Henry's law. COD was determined using the precast reagent tubes. The concentrations of nitrate and nitrite were measured using the ultraviolet spectrophotometry. A SPSS software was used to analyze the experimental data, and $p < 0.05$ is regarded as statistically significant.

CRediT authorship contribution statement

Suwan Dai: Writing – review & editing, Writing – original draft, Methodology, Conceptualization. **Haixiao Guo:** Methodology, Investigation. **Yiming Li:** Validation, Investigation. **Jiaqi Hou:** Validation. **Yufen Wang:** Supervision. **Tingting Zhu:** Resources, Methodology. **Bing-Jie Ni:** Project administration, Methodology. **Yiwen Liu:** Validation, Supervision, Resources, Project administration, Conceptualization.

Declaration of competing interest

The authors declare that they have no known competing financial interests or personal relationships that could have appeared to influence the work reported in this paper.

Acknowledgments

This study was funded by the National Natural Science Foundation of China through projects No 52470108 and 52000135.

Supplementary materials

Supplementary material associated with this article can be found, in

the online version, at doi:10.1016/j.wroa.2024.100275.

Data availability

Data will be made available on request

References

Bai, Y.M., Mao, J., Li, D.X., Luo, X.J., Chen, J., Tay, F.R., Niu, L.N., 2019. Bimodal antibacterial system based on quaternary ammonium silane-coupled core-shell hollow mesoporous silica. Acta Biomater. 85, 229–240.

Baker, A., 2002. Fluorescence excitation-Emission matrix characterization of river waters impacted by a tissue mill effluent. Environ. Sci. Technol. 36 (7), 1377–1382.

Campos, O.A., Attar, N., Cheng, C., Vogelauer, M., Mallipeddi, N.V., Schmollinger, S., Matulionis, N., Christofk, H.R., Merchant, S.S., Kurdistani, S.K., 2021. A pathogenic role for histone H3 copper reductase activity in a yeast model of Friedreich's ataxia. Sci. Adv. 7 (51), eabj9889.

Chen, Q., Zhao, K., Li, G., Luo, J., Li, X., Zeng, Y., Wang, X.M., 2022. Highly permeable polylactic acid membrane grafted with quaternary ammonium salt for effective and durable water disinfection. ACS Appl. Mater. Interface. 14 (38), 43741–43748.

Du, B., Wang, S., Chen, G., Wang, G., Liu, L., 2022. Nutrient starvation intensifies chlorine disinfection-stressed biofilm formation. Chemosphere 295, 133827.

Etim, I.-I.N., Dong, J., Wei, J., Nan, C., Daniel, E.F., Subedi, D.B., Xu, D., Yadav, A.P., Su, M., Ke, W., 2020. Mitigation of sulphate-reducing bacteria attack on the corrosion of 20SiMn steel rebar in sulphoaluminate concrete using organic silicon quaternary ammonium salt. Construct. Build. Mater. 257, 119047.

Guo, H., Liu, S., Wang, Y., Wang, Y., Hou, J., Zhu, T., Liu, Y., 2023a. Reduced sulfide and methane in rising main sewer via calcium peroxide dosing: insights from microbial physiological characteristics, metabolisms and community traits. J. Hazard. Mater. 451, 131138.

Guo, H., Tian, L., Liu, S., Wang, Y., Hou, J., Zhu, T., Liu, Y., 2023b. The potent effects of polyoxometalates (POMs) on controlling sulfide and methane production from sewers. Chem. Eng. J. 453, 139955.

He, Y., Li, Y., Li, X., Liu, Y., Wang, Y., Guo, H., Hou, J., Zhu, T., Liu, Y., 2023. Net-zero greenhouse gas emission from wastewater treatment: mechanisms, opportunities and perspectives. Renew. Sustain. Energy Rev. 184, 113547.

He, Y., Liu, Y., Li, X., Guo, H., Zhu, T., Liu, Y., 2024. Polyvinyl chloride microplastics facilitate nitrous oxide production in partial nitritation systems. Environ. Sci. Technol. 58 (4), 1954–1965.

Jaillard, M., van Belkum, A., Cady, K.C., Creely, D., Shortridge, D., Blanc, B., Barbu, E.M., Dunne Jr., W.M., Zambardi, G., Enright, M., Mugnier, N., Le Priol, C., Schicklin, S., Guigon, G., Veyrieras, J.B, 2017. Correlation between phenotypic antibiotic susceptibility and the resistome in Pseudomonas aeruginosa. Int. J. Antimicrob. Agent. 50 (2), 210–218.

Jiang, G., Keating, A., Corrie, S., O'Halloran, K., Lam, N., Yuan, Z., 2013. Dosing free nitrous acid for sulfide control in sewers: results of field trials in Australia. Water Res. 47 (13), 4331–4339.

Kobylinski, E., Neun, G., Massart, N., Lokken, T., Myers, E., 2007. A tale of two filaments: BNR system recovery from a major process upset. In: Proceedings of the Water Environment Federation, pp. 8428–8449.

Kobylinski, E., Durme, G., Barnard, J., Massart, N., Koh, S.H., 2008. How biological phosphorous removal is inhibited by collection system corrosion and odor control practices. In: Proceedings of the Water Environment Federation, pp. 1719–1735.

Kobylinski, E., Durme, G.P., Barnard, J., Shaw, A., Steichen, M.T., 2010. Impact of odor and corrosion control practices on the influent readily biodegradable COD fraction and biological nutrient removal system performance. In: Proceedings of the Water Environment Federation, pp. 7612–7635.

Li, J., Ahmed, W., Metcalfe, S., Smith, W.J.M., Choi, P.M., Jackson, G., Cen, X., Zheng, M., Simpson, S.L., Thomas, K.V., Mueller, J.F., Thai, P.K., 2023. Impact of sewer biofilms on fate of SARS-CoV-2 RNA and wastewater surveillance. Nat. Water 1, 272–280.

Li, Y., Yang, F., Miao, S., Wang, D., Li, Z., Yuan, X., Yuan, L., Liu, Q., 2021. Achieved deep-dewatering of dredged sediments by Fe(II) activating persulfate pretreatment: filtrating performance and mechanistic insights. Chem. Eng. J. 405, 126847.

Li, Y., Zhu, Y., Wang, D., Yang, G., Pan, L., Wang, Q., Ni, B.-J., Li, H., Yuan, X., Jiang, L., Tang, W., 2020. Fe(II) catalyzing sodium percarbonate facilitates the dewaterability of waste activated sludge: performance, mechanism, and implication. Water Res. 174, 115626.

Liu, M., Rashid, S., Wang, W., Zhang, H., Zhao, Y., Fu, X., Su, Z., Graham, N., Yu, W., 2024. The application of chitosan quaternary ammonium salt to replace polymeric aluminum ferric chloride for sewage sludge dewatering. Water Res. 256, 121539.

Liu, Y., Qiu, S., Wang, N., Ma, R., Liang, J., 2023. Study on rapid start-up and stable nitrogen removal efficiency of carrier enhanced continuous flow PD/A granular sludge system. J. Environ. Chem. Eng. 11 (6), 111268.

Subair, A., Lakshmi, P.K., Chellappan, S., Chinghakham, C., 2024. Removal of polystyrene microplastics using biochar-based continuous flow fixed-bed column. Environ. Sci. Pollut. Res. 31 (9), 13753–13765.

Unnikrishnan, A., Das, P., Thakur, N.L., Devi, P., 2024. Exploring the depths: metagenomic profiling of cold seep bacterial communities and isolation of hydrocarbon-degrading microbes from the Cauvery-Mannar basin. Region. Stud. Marine Sci. 72, 103440.

USEPA, 2007. Reregistration Eligibility Decision for Trimethoxysilyl Quaternary Ammonium Chloride Compounds, 739-R-07-007.

Usman, M., Shi, Z., Cai, Y., Zhang, S., Luo, G., 2023. Microbial insights towards understanding the role of hydrochar in enhancing phenol degradation in anaerobic digestion. Environ. Pollut. 330, 121779.

Vereshchagin, A.N., Frolov, N.A., Egorova, K.S., Seitkalieva, M.M., Ananikov, V.P., 2021. Quaternary Ammonium Compounds (QACs) and ionic liquids (ILs) as biocides: from simple antiseptics to tunable antimicrobials. Int. J. Mol. Sci. 22 (13), 6793.

Wang, Y., Guo, H., Li, X., Chen, X., Peng, L., Zhu, T., Sun, P., Liu, Y., 2024. Peracetic acid (PAA)-based pretreatment effectively improves medium-chain fatty acids (MCFAs) production from sewage sludge. Environ. Sci. Ecotechnol. 20, 100355.

Wang, Y., Zheng, K., Guo, H., Tian, L., He, Y., Wang, X., Zhu, T., Sun, P., Liu, Y., 2023. Potassium permanganate-based advanced oxidation processes for wastewater decontamination and sludge treatment: a review. Chem. Eng. J. 452, 139529.

Wang, Y., Zheng, K., Guo, H., Tong, Y., Zhu, T., Liu, Y., 2022. Unveiling the mechanisms of how vivianite affects anaerobic digestion of waste activated sludge. Bioresour. Technol. 343, 126045.

Wang, Z., Gao, M., Wang, S., Xin, Y., Ma, D., She, Z., Wang, Z., Chang, Q., Ren, Y., 2014. Effect of hexavalent chromium on extracellular polymeric substances of granular sludge from an aerobic granular sequencing batch reactor. Chem. Eng. J. 251, 165–174.

Wei, H., Gao, B., Ren, J., Li, A., Yang, H., 2018. Coagulation/flocculation in dewatering of sludge: a review. Water Res. 143, 608–631.

Xu, N., Li, H., Guo, T., Hou, Y., Han, Y., Song, Y., Zhang, D., Guo, J., 2023. Effect of ibuprofen on the sulfur autotrophic denitrification process and microbial toxic response mechanism. Bioresour. Technol. 384, 129261.

Yan, X., Sun, J., Kenjiahan, A., Dai, X., Ni, B.-J., Yuan, Z., 2020. Rapid and strong biocidal effect of ferrate on sulfidogenic and methanogenic sewer biofilms. Water Res. 169, 115208.

Yin, F., Wei, H., Yue, X., Tan, H., Yang, X., Lu, S., Wang, S., Zhao, Y., Liu, H., 2024. Fast circulatory nitrification/denitrification process using continuous flow synchronous settling reactors promotes organic utilization efficiency in nitrogen removal. Chem. Eng. J. 489, 151242.

You, F., Tang, M., Zhang, J., Wang, D., Fu, Q., Zheng, J., Ye, B., Zhou, Y., Li, X., Yang, Q., Liu, X., Duan, A., Liu, J., 2024. Benzethonium chloride affects short chain fatty acids produced from anaerobic fermentation of waste activated sludge: performance, biodegradation and mechanisms. Water Res. 250, 121024.

You, G., Wang, P., Hou, J., Wang, C., Xu, Y., Miao, L., Lv, B., Yang, Y., Liu, Z., Zhang, F., 2017. Insights into the short-term effects of CeO_2 nanoparticles on sludge dewatering and related mechanism. Water Res. 118, 93–103.

Zan, F., Tang, W., Jiang, F., Chen, G., 2021. Diversion of food waste into the sulfate-laden sewer: interaction and electron flow of sulfidogenesis and methanogenesis. Water Res. 202, 117437.

Zhang, L., Qiu, Y.-Y., Sharma, K.R., Shi, T., Song, Y., Sun, J., Liang, Z., Yuan, Z., Jiang, F., 2023. Hydrogen sulfide control in sewer systems: a critical review of recent progress. Water Res. 240, 120046.

Zhou, Z., Zhang, X., Zeng, S., Xu, Y., Nie, W., Zhou, Y., Chen, P., 2024. Quaternary ammonium salts for water treatment with balanced rate of sterilization and degradation. Chemosphere 352, 141386-141386.

Zhu, L., Ma, J., Yuan, H., Deng, L., Shi, Z., He, Q., Ke, S., 2023. Effects of successional sulfadiazine exposure on biofilm in moving bed biofilm reactor: secretion of extracellular polymeric substances, community activity and functional gene expression. Bioresour. Technol. 380, 129092.

Zuo, Z., Song, Y., Ren, D., Li, H., Gao, Y., Yuan, Z., Huang, X., Zheng, M., Liu, Y., 2020. Control sulfide and methane production in sewers based on free ammonia inactivation. Environ. Int. 143, 105928.

Zuo, Z., Xing, Y., Liu, T., Zheng, M., Lu, X., Chen, Y., Jiang, G., Liang, P., Huang, X., Liu, Y., 2024. Methane mitigation via the nitrite-DAMO process induced by nitrate dosing in sewers. Water Res. 257, 121701.